Electron transmission through bilayer graphene: A time-dependent first-principles study

Hironari Miyauchi, Yoshihiro Ueda, Yasumitsu Suzuki, and Kazuyuki Watanabe*
Department of Physics, Tokyo University of Science, 1-3 Kagurazaka, Shinjuku-ku, Tokyo 162-8601, Japan
(Received 26 January 2017; published 17 March 2017)

Incident-energy-dependent electron transmittances through single-layer graphene (SLG) and bilayer graphene (BLG) were investigated using time-dependent density functional theory. The transmittances of BLG with two kinds of stacking exhibit an unexpected crossing at a certain incident electron energy. The behavior is preserved for the BLG with reduced or increased layer distances compared to that of typical BLG. We determined the origin of the crossing by investigating transmission electron diffraction patterns for SLG.

DOI: 10.1103/PhysRevB.95.125425

I. INTRODUCTION

Many layered materials have been synthesized and have attracted a great deal of attention, since they have a number of intriguing physical properties that are of interest for fundamental physics and important applications [1]. Among the various layered materials, e.g., hexagonal boron nitride, silicene, transition metal dichalcogenides, and metal halides, graphene is the simplest atomically thin hexagonal sheet [2]. The atomic and electronic structures of graphene and few-layer graphene have been analyzed by low-energy electron scattering (LEES) [3]. The reflectivity of graphene for low-energy electrons has proven to be a very useful probe of the material [4,5]. Transmission electron through graphene using a low-energy electron point source microscopy is also important for probing the electronic structure and imaging the material [6,7].

Bilayer graphene (BLG), in particular, has been the focus of numerous LEES studies [8] due to its unique low-energy band structure, which can be altered using a transverse electric field or by applying mechanical strain [2]. LEES by BLG is a fundamental but challenging research topic, not only because the low-energy electrons capture both the electronic and atomic structures very precisely, but also because the microscopic mechanism of LEES by BLG is in itself unknown. Regarding theoretical LEES analysis of layered materials, a time-domain simulation of electron diffraction in crystals by Yan *et al.* [9] gave reasonable transmission electron microscopy images and low-energy electron diffraction (LEED) intensities for graphene and bulk silicon using an electron wave packet (WP). Very recently, time-dependent density functional theory (TDDFT) [10–12] simulations have been applied to LEES by graphene flakes. The study successfully determined nano-LEED patterns and found π and $\pi + \sigma$ plasmon oscillations [13] of and secondary electron emission (SEE) from the target [14].

Motivated by these LEES studies on layered materials, we theoretically explored the electron transmittance of BLG by TDDFT using a similar technique to that of previous studies [13,14]. The objectives of the present study are to calculate incident-energy-dependent and stacking-type-dependent transmittances of BLG and to elucidate the underlying mechanism of LEES by BLG. We found an unexpected crossing between the energy-dependent transmittances of AA-stacked and AB-stacked BLG, and interpreted this feature based on transmission electron diffraction patterns for single-layer graphene (SLG).

II. MODEL AND METHOD

The computational framework is similar to those of previous studies [13,14] that have been developed for simulating nano-LEED and SEE for nanographene upon electron impact. The nanographene scattering target was a hydrogen-terminated flake (a circumcoronene, $C_{54}H_{18}$), the incident electron was a finite-sized WP in three-dimensional space, and the calculation was performed in real time and real space. In the present study, however, we need to calculate the transmittance of BLG with a high accuracy and without the influence of finite-sized (or edge) effects caused by both the target flake and the incident WP. Therefore, we implemented into our plane-wave-based TDDFT program [15] a model in which the BLG target and incident WP are infinitely long in the direction parallel to the target plane with periodic boundary conditions.

Figure 1 shows the structures of the graphene targets investigated in this study. The layer distances of AA-stacked and AB-stacked BLG are 3.35 Å. We shoot an electron at each of these three structures and study the scattering dynamics. A schematic view of our calculation unit cell is shown in Fig. 2.

Here, an incident free electron is expressed as a WP with a Gaussian envelope along the x direction and is uniform along the y and z directions. The electron is shot from the negative side of the target along the x axis toward the positive direction.

The computation is conducted in the following way. First, we determine the ground state for the target using density functional theory (DFT) [16,17]. Then, the one-particle wave function that corresponds to the incident WP is added to the system and expressed as

$$\psi_{\mathrm{WP},\mathbf{k}=\Gamma}(\mathbf{r}) = \left(\frac{1}{\pi\sigma^2}\right)^{\frac{1}{4}} \exp\left[-\frac{(x-x_0)^2}{2\sigma^2} + ik_0(x-x_0)\right], \tag{1}$$

where σ, x_0, k_0 are the standard deviation, center position, and wave vector for the initial WP, respectively. (We adopt atomic units throughout the paper, unless stated otherwise.) In the actual computation, the Fourier transform of Eq. (1) is used. We note that the present ψ_{WP} is nonzero only at the Γ point, and it is normalized so that the number of electrons that belongs to

*kazuyuki@rs.kagu.tus.ac.jp

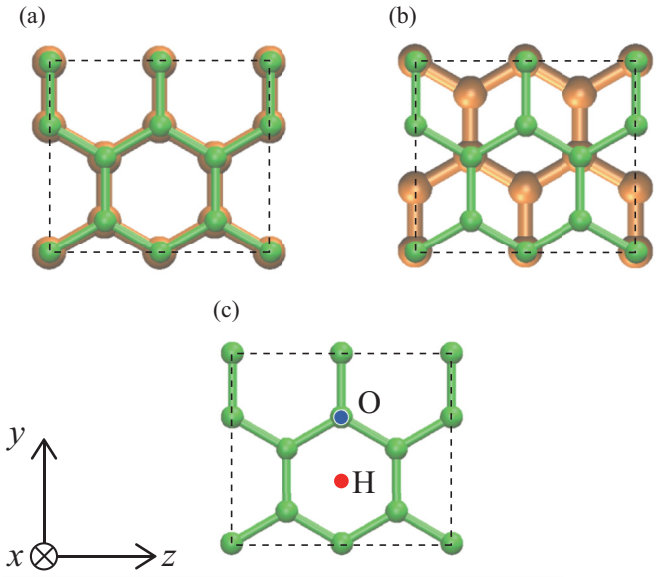

FIG. 1. Structures of graphene targets: (a) AA-stacked BLG, (b) AB-stacked BLG, and (c) SLG. The dashed lines indicate the calculation unit cell. Panel (c) shows two observation points for transmission electron diffraction intensity, O (on-top site) and H (hollow site), which are a few angstroms from the SLG (see text) and projected onto the SLG plane.

the WP is 1. Since the system is charged by adding the electron WP to the calculation unit cell, the DFT calculation is not carried out for the initial state. Instead, the time evolution of the whole electronic states without diagonalizing the Hamiltonian is determined as follows. The wave functions $\psi_{i,\mathbf{k}}(\mathbf{r},t)$ and $\psi_{\mathrm{WP},\mathbf{k}}(\mathbf{r},t)$ for the target and incident WP at $t = 0$, respectively, are evolved in time according to the time-dependent Kohn-Sham (TDKS) equation:

$$i\frac{\partial}{\partial t}\psi_{i,\mathbf{k}}(\mathbf{r},t) = H_{\mathrm{TDKS}}[n(\mathbf{r},t)]\psi_{i,\mathbf{k}}(\mathbf{r},t), \tag{2}$$

$$i\frac{\partial}{\partial t}\psi_{\mathrm{WP},\mathbf{k}}(\mathbf{r},t) = H_{\mathrm{TDKS}}[n(\mathbf{r},t)]\psi_{\mathrm{WP},\mathbf{k}}(\mathbf{r},t), \tag{3}$$

and

$$n(\mathbf{r},t) = \frac{1}{N_k}\sum_{\mathbf{k}}\left[2\sum_{i=1}^{N/2}\left|\psi_{i,\mathbf{k}}(\mathbf{r},t)\right|^2 + \left|\psi_{\mathrm{WP},\mathbf{k}}(\mathbf{r},t)\right|^2\right], \tag{4}$$

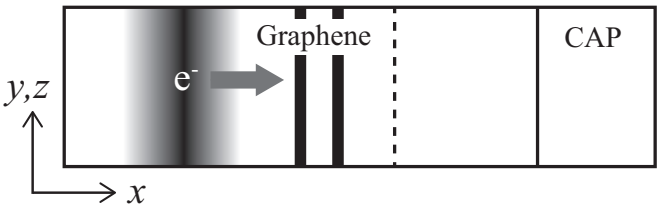

FIG. 2. Schematic view of the calculation unit cell. The initial position of the WP is 10.6 Å from the target. The plane indicated by a dashed line is the observation plane for the electron transmittance calculation. A complex absorbing potential (CAP) is placed at the boundary of the positive x direction.

where $\mathbf{k}$ is the wave vector, i runs from 1 to $N/2$ (N is the number of electrons in the target), N_k is a number of sampled $\mathbf{k}$ points, and the system is assumed to be spin unpolarized. As time evolves, the incident electron gradually interacts with the target electrons. Here, the interaction between electrons is not exact in that it does not include the exact exchange-correlation potential but one approximated using the adiabatic local density approximation [14,18].

The computational details are as follows. The size of the calculation unit cell (shown in Figs. 1 and 2) is $52.9 \times 4.3 \times 4.9\,\text{Å}^3$. We set the kinetic energy of the incident WP as $E_{\mathrm{kin}} = k_0^2/2 = 60$–$300$ eV and its width as $\sigma = 3.0$ Å. The initial distance, 10.6 Å, of the WP from the target is large enough that there is no overlap between the wave functions. The time evolution of the KS wave functions is explored using a fourth-order Taylor expansion method [19], and we use a time step of $\Delta t = 2.42 \times 10^{-4}$ fs. For the basis set, a plane-wave expansion is used together with a norm-conserving pseudopotential [20,21]. N_k is 16 including the Γ point, and the cutoff energy is 537 eV. During the simulation, the atomic positions are fixed because the time interval is too short to see the atomic motion. A complex absorbing potential (CAP) [22,23], the width of which is 10.0 Å, is placed at the boundary of the positive x direction of the calculation unit cell.

To quantitatively understand the electron scattering dynamics that are determined by the equations above, we calculate and discuss two physical quantities. One is the transmittance, expressed by

$$T = |J_{\mathrm{S}}|/|J_{\mathrm{incident}}|, \tag{5}$$

where

$$J_{\mathrm{S}} = \frac{1}{N_k}\sum_{\mathbf{k}}\int_{t_1}^{t_2} dt \int_{\mathrm{S}} dS\left\{2\sum_{i=1}^{\mathrm{N/2}}[\psi_{i,\mathbf{k}}^*\nabla\psi_{i,\mathbf{k}} - (\nabla\psi_{i,\mathbf{k}}^*)\psi_{i,\mathbf{k}}] + [\psi_{\mathrm{WP},\mathbf{k}}^*\nabla\psi_{\mathrm{WP},\mathbf{k}} - (\nabla\psi_{\mathrm{WP},\mathbf{k}}^*)\psi_{\mathrm{WP},\mathbf{k}}]\right\} \tag{6}$$

is the number of electrons passing through the fixed observation plane S (shown as a dashed line in Fig. 2). Here, t_1 and t_2 are the starting and ending times for the simulation, respectively. The transmittance T is obtained by normalizing J_{S} by the initial number of incident electrons $|J_{\mathrm{incident}}|$, which is 1 in this simulation.

The other is the intensity of the diffraction pattern $I(\mathbf{r})$. It is calculated by

$$I(\mathbf{r}) = \frac{N(\mathbf{r})}{N_{\mathrm{freespace}}(\mathbf{r})}, \tag{7}$$

where

$$N(\mathbf{r}) = \int_{t_1}^{t_2} n(\mathbf{r},t)dt, \quad \mathbf{r} \in \mathrm{S}' \tag{8}$$

is the time-integrated total electron density $n(\mathbf{r},t)$ at point $\mathbf{r}$ on the observation plane S′. To obtain $I(\mathbf{r})$, $N(\mathbf{r})$ is normalized with respect to the free space transmitted intensity $N_{\mathrm{freespace}}(\mathbf{r})$, which is obtained in another simulation where the graphene target is absent. The diffraction pattern $I(\mathbf{r})$ is calculated for

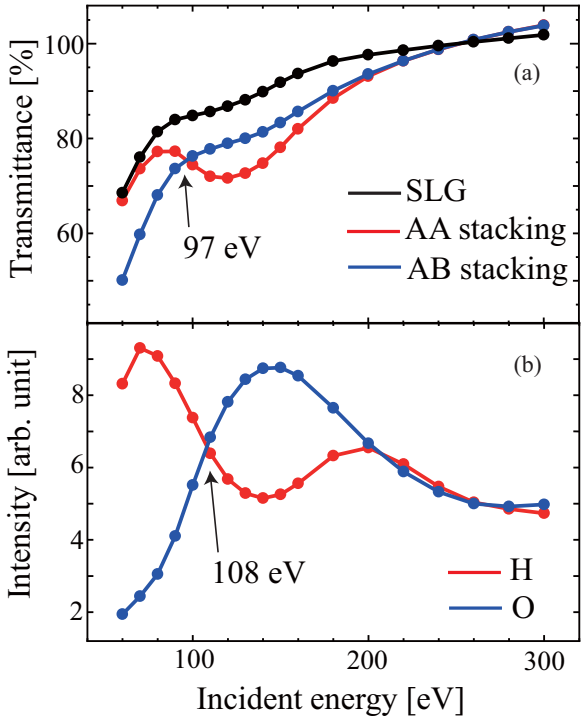

FIG. 3. (a) Energy-dependent electron transmittance depending on the stacking type: SLG (black line), AA-stacked BLG (red line), and AB-stacked BLG (blue line). (b) Energy-dependent transmission electron diffraction intensity of SLG at the H site (red line) and O site (blue line) (at a distance of 3.35 Å from the target).

the SLG [Fig. 1(c)]. While the position of the observation plane S (which is used to calculate the transmittance) is fixed, the position of S′ is varied in the analysis.

III. RESULTS AND DISCUSSION

The transmittances [Eq. (5)] of SLG and AA- and AB-stacked BLG as a function of incident electron energy are given in Fig. 3(a). The profile of the curve for SLG (black solid line with dots) differs from that obtained in a previous study [9], because their data were generated with a monochromatic wave constructed from the Fourier transform of the incident electron WP. In contrast, our incident electron WP has a finite width along the x direction and thus is not monochromatic. We confirmed that the profile becomes more undulant in energy as the width (σ) of the WP increases, or equivalently, with a more monochromatic wave. Otherwise, the present value ranging from ∼70% to ∼95% in the energy of 60–200 eV, which is shown in Fig. 3(a), is in agreement with those obtained in the study [9] and is also compatible with the value of ∼74% in the energy range of 100–200 eV in the previous experiment [7].

In the high-energy region, the three curves approach 100%. This is physically reasonable, because a high-energy electron that is transmitted through the first layer cannot see the difference in the potential barrier between the two types of stacking. The curves even exceed 100% at around 240 eV, because high-energy incident electrons cause SEE, which has been discussed in the previous study [14]. In contrast, the

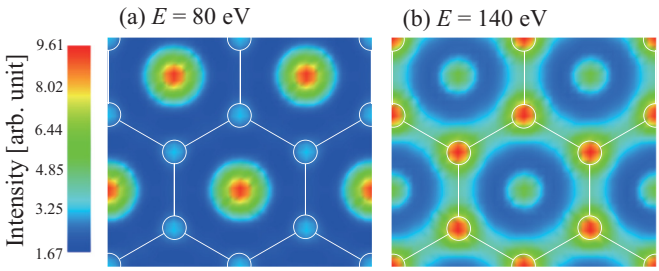

FIG. 4. Transmission electron diffraction patterns for (a) E = 80 eV and (b) E = 140 eV at a distance of 3.35 Å from the SLG. White thin lines and open circles correspond to C-C bonds and carbon atoms of the target, respectively.

three curves deviate from each other in the low-energy region; the transmittances of SLG and AB-stacked BLG increase monotonically with increasing incident energy, whereas that of AA-stacked BLG dips once after increasing and then again increases. The curves for AB- and AA-stacked BLG cross at 97 eV. The features of the transmittance in the low-energy region are unexpected.

To investigate the origin of the crossing, we calculated the transmission electron diffraction intensity [Eq. (7)] for SLG at the hollow site (H) and at the on-top site (O) on a plane a distance of 3.35 Å (typical BLG layer distance) from the SLG in the positive x direction [shown in Fig. 1(c)], which corresponds to the Fresnel diffraction regime [24]. When a periodic object is illuminated with monochromatic light or an electron wave, a self-image of the object is formed at finite distances from the object. This self-imaging phenomenon is known as the Talbot effect [25,26], which arises as a result of Fresnel diffraction [24]. We note that the diffraction patterns in our calculation are not due to the Talbot effect but to Fresnel diffraction in the strict sense, because the present incident electron is not monochromatic. The diffraction intensities at the H and O sites are given as a function of incident electron energy in Fig. 3(b). Very interestingly, the diffraction intensities at the O and H sites in the low-energy region exhibit an energy dependence similar to the transmittances for AB- and AA-stacked BLG shown in Fig. 3(a), respectively. In particular, the two curves cross at 108 eV. To clearly see the difference between the intensities at higher and lower energies than the crossing point, the distributions of diffraction intensity for incident energies of 80 eV and 140 eV, which are respectively below and above the crossing energy, are drawn in Fig. 4. The intensities are largest at the H and O sites for (a) 80 eV and (b) 140 eV, respectively. Since the wavelength of the incident electrons depends on their energy, the diffraction patterns vary with the incident energy [9]. Having found the relevance between the transmittance of BLG and diffraction of SLG, we can interpret the stacking-type dependence of the transmittance as follows.

Figure 5 is a schematic view of the diffraction intensities and transmittances for AA- and AB-stacked BLG at incident energies of (a) 80 eV and (b) 140 eV. Black solid lines and dots represent graphene layers and carbon atoms, respectively. An electron is shot from the negative side of the BLG in Fig. 5. Filled thick and thin arrows between the layers signify high and low diffraction intensities, respectively, after

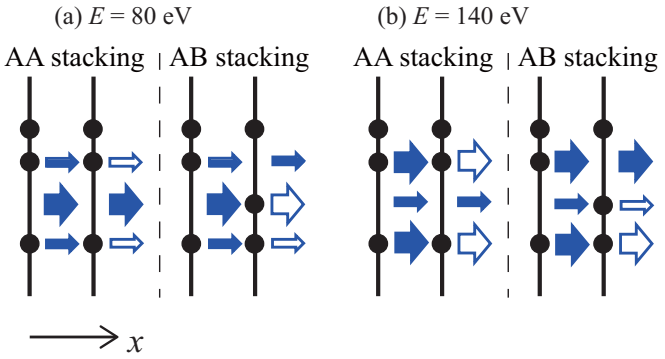

FIG. 5. Schematic illustrations of electron transmission for (a) $E = 80$ eV and (b) $E = 140$ eV incidence. The size of the arrows between the layers indicates the diffraction intensity at the position of the second layer. The energy-dependent transmittance of BLG is determined by the diffraction intensity distribution and stacking type (AA or AB).

transmission through the first layer. Filled and open arrows on the right side of the second layer signify unchanged and reduced diffraction intensities, respectively, after transmission through the second layer. The transmittance is evaluated by summing the magnitude of the arrows on the positive side of the second layer. For 80-eV incidence [in Fig. 5(a)] at the first layer, the diffraction intensity is largest at the H sites on the corresponding second layer [in Fig. 4(a)], where there are carbon atoms in the second layer of AB stacking, which are obstacles for transmission. Thus, the transmission through the second layer of AB-stacked BLG is heavily suppressed, as shown by the open arrow [AB-stacking case of (a)]. In contrast, for AA stacking, since there are no carbon atoms in the second layer corresponding to H sites, the transmittance is not reduced [AA-stacking case in (a)]. On the other hand, for the case of 140-eV incidence [in Fig. 5(b)], the diffraction intensity is largest at the O sites [in Fig. 4(b)]. Thus, the situation is inverted from the case of 80-eV incidence, resulting in the opposite relationship for the transmittance magnitude between AA- and AB-stacked BLG.

To check if the relationship obtained above for BLG with a graphite gap of 3.35 Å holds for other distances, we repeated the transmittance calculations for different bilayer distances and diffraction intensities by changing the observation points accordingly. The transmittances for a small distance of 2.79 Å and a large distance of 3.91 Å are given in Figs. 6(a) and 6(c), respectively. The corresponding diffraction intensities are given in Figs. 6(b) and 6(d). A clear relationship in the crossing behavior between the transmittance and diffraction intensity at a certain energy is observed. These results guarantee the validity of interpreting the stacking-type-dependent transmittance of BLG using the SLG diffraction intensity.

Last, we consider the reason why the crossing point energies in the transmission and diffraction spectra do not exactly coincide with each other, as can be seen in Figs. 3 and 6. The diffraction intensity reflects single scattering by SLG, while the transmittance is the sum of the probabilities for various types of multiscattering in addition to forward scattering through the first and second layers. Therefore, it is clear that the

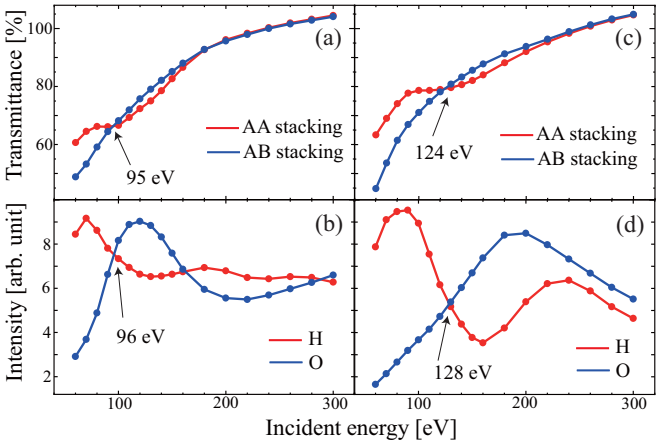

FIG. 6. Electron transmittance as a function of incident electron energy for AA-stacked (red line) and AB-stacked BLG (blue line). Interlayer distances are (a) 2.79 Å and (c) 3.91 Å. Transmission diffraction intensity as a function of incident electron energy for SLG calculated at distances of (b) 2.79 Å and (d) 3.91 Å from the target.

energies in question do not necessarily coincide with each other. Nevertheless, crossing at these energies exists for both the BLG transmittance and SLG diffraction intensity. This is because direct forward scattering dominates the transmission path for the bilayer for low-energy (∼100 eV) electron incidence.

The crossover in transmittance that we have found and discussed in the present study has been observed neither experimentally nor theoretically, and thus is a theoretical prediction, as far as we know. Detailed studies on electron scattering by few-layer graphene and other layered materials, especially by experiments, are desirable.

IV. CONCLUSION

We investigated electron scattering by AA-stacked and AB-stacked BLG using TDDFT and obtained energy-dependent transmittances that exhibit an unexpected crossing. The crossing behavior is successfully interpreted using the diffraction intensity distribution of SLG. Importantly, the crossing behavior holds for simulated BLG with reduced or increased layer distances compared with the real graphite gap. The present study not only revealed the close relationship between BLG transmittance and SLG diffraction for LEES, but also provides relevant knowledge that will be useful for various surface analysis techniques based on electron scattering spectroscopy.

ACKNOWLEDGMENTS

K.W. is supported by JSPS KAKENHI Grant No. JP16K05483. Y.S. is supported by JSPS KAKENHI Grant No. JP16K17768. Numerical calculations were performed on the supercomputers of the Institute for Solid State Physics, The University of Tokyo and at the Research Center for Computational Science, National Institutes of Natural Sciences, Okazaki Research Facilities in Japan.

[1] S. Z. Butler, S. M. Hollen, L. Cao, Y. Cui, J. A. Gupta, H. R. Gutiérrez, T. F. Heinz, S. S. Hong, J. Huang, A. F. Ismach *et al.*, ACS Nano **7**, 2898 (2013).
[2] A. C. Ferrari, F. Bonaccorso, V. Fal'ko, K. S. Novoselov, S. Roche, P. Boggild, S. Borini, F. H. L. Koppens, V. Palermo, N. Pugno *et al.*, Nanoscale **7**, 4598 (2015).
[3] J.-N. Longchamp, T. Latychevskaia, C. Escher, and H.-W. Fink, Appl. Phys. Lett. **101**, 113117 (2012).
[4] H. Hibino, H. Kageshima, F. Maeda, M. Nagase, Y. Kobayashi, and H. Yamaguchi, Phys. Rev. B **77**, 075413 (2008).
[5] R. M. Feenstra, N. Srivastava, Q. Gao, M. Widom, B. Diaconescu, T. Ohta, G. L. Kellogg, J. T. Robinson, and I. V. Vlassiouk, Phys. Rev. B **87**, 041406 (2013).
[6] F. Wicki, J.-N. Longchamp, T. Latychevskaia, C. Escher, and H.-W. Fink, Phys. Rev. B **94**, 075424 (2016).
[7] J. Y. Mutus, L. Livadaru, J. T. Robinson, R. Urban, M. H. Salomons, M. Cloutier, and R. A. Wolkow, New J. Phys. **13**, 063011 (2011).
[8] A. Rozhkov, A. Sboychakov, A. Rakhmanov, and F. Nori, Phys. Rep. **648**, 1 (2016).
[9] J.-A. Yan, J. A. Driscoll, B. K. Wyatt, K. Varga, and S. T. Pantelides, Phys. Rev. B **84**, 224117 (2011).
[10] E. Runge and E. K. U. Gross, Phys. Rev. Lett. **52**, 997 (1984).
[11] K. Burke, J. Werschnik, and E. K. U. Gross, J. Chem. Phys. **123**, 062206 (2005).
[12] C. A. Ullrich, U. J. Gossmann, and E. K. U. Gross, Phys. Rev. Lett. **74**, 872 (1995).
[13] K. Tsubonoya, C. Hu, and K. Watanabe, Phys. Rev. B **90**, 035416 (2014).
[14] Y. Ueda, Y. Suzuki, and K. Watanabe, Phys. Rev. B **94**, 035403 (2016).
[15] K. Tada and K. Watanabe, Phys. Rev. Lett. **88**, 127601 (2002).
[16] P. Hohenberg and W. Kohn, Phys. Rev. **136**, B864 (1964).
[17] W. Kohn and L. J. Sham, Phys. Rev. **140**, A1133 (1965).
[18] J. P. Perdew and A. Zunger, Phys. Rev. B **23**, 5048 (1981).
[19] K. Yabana and G. F. Bertsch, Phys. Rev. B **54**, 4484 (1996).
[20] N. Troullier and J. L. Martins, Phys. Rev. B **43**, 1993 (1991).
[21] K. Kobayashi, Comput. Mater. Sci. **14**, 72 (1999).
[22] D. E. Manolopoulos, J. Chem. Phys. **117**, 9552 (2002).
[23] T. Gonzalez-Lezana, E. J. Rackham, and D. E. Manolopoulos, J. Chem. Phys. **120**, 2247 (2004).
[24] J. T. Winthrop and C. R. Worthington, J. Opt. Soc. Am. **55**, 373 (1965).
[25] J. Wen, Y. Zhang, and M. Xiao, Adv. Opt. Photon. **5**, 83 (2013).
[26] J. A. Salas, K. Varga, J.-A. Yan, and K. H. Bevan, Phys. Rev. B **93**, 104305 (2016).